

Large-Scale Structure and Hyperuniformity of Amorphous Ices

Fausto Martelli,^{1,*} Salvatore Torquato,^{1,2} Nicolas Giovambattista,^{3,4} and Roberto Car^{1,2}

¹*Department of Chemistry, Princeton University, Princeton, New Jersey, USA*

²*Department of Physics, Princeton University, Princeton, New Jersey, USA*

³*Department of Physics, Brooklyn College of the City University of New York, New York, New York, USA*

⁴*Ph.D. Programs in Chemistry and Physics, The Graduate Center of the City University of New York, New York, New York 10016, USA*

(Received 26 April 2017; published 29 September 2017)

We investigate the large-scale structure of amorphous ices and transitions between their different forms by quantifying their large-scale density fluctuations. Specifically, we simulate the isothermal compression of low-density amorphous ice (LDA) and hexagonal ice to produce high-density amorphous ice (HDA). Both HDA and LDA are nearly hyperuniform; i.e., they are characterized by an anomalous suppression of large-scale density fluctuations. By contrast, in correspondence with the nonequilibrium phase transitions to HDA, the presence of structural heterogeneities strongly suppresses the hyperuniformity and the system becomes hyposurficial (devoid of “surface-area fluctuations”). Our investigation challenges the largely accepted “frozen-liquid” picture, which views glasses as structurally arrested liquids. Beyond implications for water, our findings enrich our understanding of pressure-induced structural transformations in glasses.

DOI: 10.1103/PhysRevLett.119.136002

Introduction.—Disordered hyperuniform materials are exotic amorphous states of matter that lie between a crystal and a liquid: they are like perfect crystals in the way they suppress large-scale density fluctuations and are like liquids or glasses in that they are statistically isotropic with no Bragg peaks [1]. Central to the concept of hyperuniformity is the structure factor $S(\mathbf{k})$, which, in the thermodynamic limit, is related to $\tilde{h}(\mathbf{k})$, the Fourier transform of the total correlation function $h(\mathbf{r})$, $S(\mathbf{k}) = 1 + \rho\tilde{h}(\mathbf{k})$. In d -dimensional Euclidean space, \mathbb{R}^d ($d = 3$ in this work), the number variance $\sigma^2(R)$ of particles inside a spherical window of radius R is related to $S(\mathbf{k})$ via [1]

$$\sigma^2(R) = \langle N(R) \rangle \left(\frac{1}{(2\pi)^d} \int_{\mathbb{R}^d} S(\mathbf{k}) \tilde{\alpha}(\mathbf{k}; R) d\mathbf{k} \right), \quad (1)$$

where $\langle N(R) \rangle$ is the average number of particles inside the spherical window and $\tilde{\alpha}(\mathbf{k}; R)$ is the Fourier transform of $\alpha(\mathbf{r}; R)$, defined as the volume common to two spherical windows with centers separated by a vector \mathbf{r} , divided by the volume of the window [see Eq. (S1) in Supplemental Material (SM) [2]]. For a large class of ordered and disordered systems, the number variance has the following large- R asymptotic behavior [1,3],

$$\sigma^2(R) = 2^d \phi \left[A \left(\frac{R}{D} \right)^d + B \left(\frac{R}{D} \right)^{d-1} + \ell \left(\frac{R}{D} \right)^{d-1} \right], \quad (2)$$

where $\phi = \rho v_1(D/2)$ is the dimensionless density, D is a characteristic length, $v_1(R)$ is the volume of the spherical window, A and B are volume and surface-area coefficients, respectively, and $\ell(R/D)^{d-1}$ represents terms of lower order than $(R/D)^{d-1}$. A and B can be expressed as

$$A = \lim_{|\mathbf{k}| \rightarrow 0} S(\mathbf{k}) = 1 + d2^d \phi \langle x^{d-1} \rangle \quad (3)$$

and

$$B = - \frac{d^2 2^{d-1} \Gamma(\frac{d}{2})}{\Gamma(\frac{d+1}{2}) \Gamma(\frac{1}{2})} \phi \langle x^d \rangle, \quad (4)$$

where $\Gamma(\cdot)$ is the gamma function, $x = r/D$, and $\langle x^d \rangle = \int_0^\infty x^d h(x) dx$ is the d th moment of $h(x)$ [4]. In a perfectly hyperuniform system [1], the non-negative volume coefficient vanishes, i.e., $A = 0$. Perfect crystals and quasicrystals are exactly hyperuniform. Disordered hyperuniform systems can be regarded to possess a “hidden” long-range order [5], and have recently been identified in many materials and systems [6–16]. On the other hand, when $A > 0$ and $B = 0$, the system is hyposurficial; examples include homogeneous Poisson point patterns and certain hard-sphere systems [1]. For $A > 0$, the ratio $H = S(0)/S(k_{\text{peak}})$, where k_{peak} is the wave number $k = |\mathbf{k}|$ at the largest peak height of the angularly averaged structure factor $S(k)$, measures qualitatively how close a system is to perfect hyperuniformity. Systems in which $H \lesssim 10^{-3}$ are deemed to be nearly hyperuniform [17].

In this Letter, we quantify the large-scale density fluctuations of the oxygen atoms of amorphous ices modeled via classical molecular dynamics simulations. The samples contain $N = 8192$ water molecules described by the classical TIP4P/2005 interaction potential [18]. Following Ref. [19], we consider low-density amorphous ice (LDA) generated by quenching the liquid at ambient conditions to a temperature of 80 K with a rate of 1 K/ns. We then produce two samples of high-density amorphous

ice (HDA) by applying pressure with a rate of 0.01 GPa/ns to LDA and to hexagonal ice (*Ih*) while keeping the temperature constant at $T = 80$ K. We refer to the HDA produced from *Ih* as HDA_{Ih} , and to the HDA produced from LDA to as HDA_{LDA} . We show that all these amorphs are nearly hyperuniform.

The nonequilibrium phase transitions (PTs) occur when the applied pressure is so large that the systems (*Ih* or LDA) lose mechanical stability. When this happens a pervasive pattern of structural heterogeneities appears, made of a highly disordered mixture, reminiscent of a spinodal decomposition, of molecules in high- and low-density local environments. The heterogeneities strongly suppress the hyperuniformity and, remarkably, the system becomes hyposurficial. We infer that hyposurficiality is caused by the spatially uncorrelated distribution of such heterogeneities. We also show that a significant suppression of large-scale density fluctuations emerges when cooling water below the temperature of freezing of the rotational motions, T_{gr} , and we elucidate the connection between molecular rotations and large-scale density fluctuations. T_{gr} is lower than the glass transition temperature T_{gt} at which the translational motions freeze.

To the best of our knowledge, hyposurficiality has never been detected before in any structural transformation. In the present context, hyposurficiality and the associated spinodal character of the transformation further supports the notion that the LDA-HDA transition is first-order like [20–23], consistent with the hypothesized presence of a second critical point in this water model [24,25]. Our findings shed light on amorphous ices, which play a pivotal role in understanding water properties, and also shed light on structural properties of general glasses. Finally, this work can stimulate experimentalists to probe $S(k)$ at small wave numbers in amorphous systems, and to design experiments to detect large-scale structural order.

Results.—At deeply supercooled conditions, water exhibits polyamorphism; i.e., it exists in more than one amorphous form. The most common forms are LDA and HDA [26–30], and a very high-density form has also been proposed to exist at even higher pressures [31]. Amorphous ices have been structurally characterized at short- and intermediate-length scale [32–34], but no study has probed their large-scale density fluctuations, even though reported experimental $S(k)$'s seem to reach very small values in the limit of $k \rightarrow 0$ [32,33].

Figures 1(a) and 1(b) show, respectively, the coefficients A and B during the *Ih*-to- HDA_{Ih} and LDA-to- HDA_{LDA} transformations. The deviation of A from 0 indicates the degree to which the system departs from hyperuniformity in light of its connection with $S(k)$ [Eq. (3)]. Classical crystals at $T = 0$ K are trivially hyperuniform and, hence, in the thermodynamic limit, $A = 0$. Our *Ih* sample is finite and at nonzero temperature. It acquires slightly larger values, $A \sim 10^{-4}$, which is also due to proton disorder. A

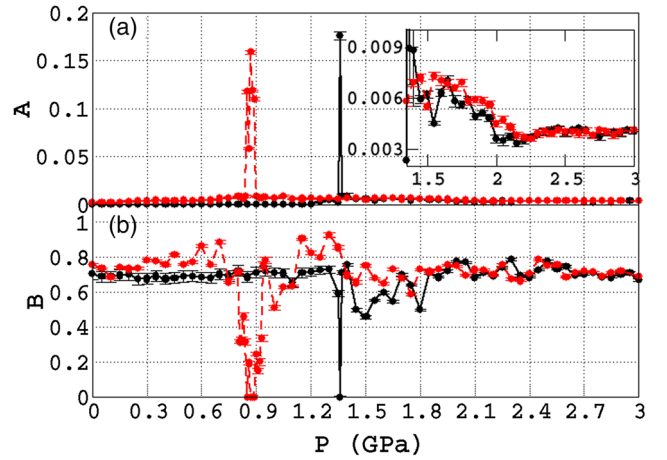


FIG. 1. (a) Coefficient A during compression of *Ih* (black, continuous) and LDA (red, dashed). Inset: zoom for $1.4 < p < 3.0$ GPa. (b) Coefficient B during compression of *Ih* (black, continuous) and LDA (red, dashed). The peaks of A signal the *Ih*-to-HDA and LDA-to-HDA transformations, in correspondence with which the system becomes hyposurficial, as shown by the sharp drop of B .

is low in LDA ($A \sim 10^{-3}$). In correspondence with the nonequilibrium PTs (at $0.85 \lesssim p_T \lesssim 1.0$ GPa in LDA, and at $1.35 \lesssim p_T \lesssim 1.36$ GPa in *Ih*), A shows a sharp peak, while B drops to almost 0 [$\lesssim 10^{-5}$, Fig. 1(b)]. We infer that hyposurficiality, as indicated by $B \rightarrow 0$, is due to the bimodal distribution of nearly uncorrelated clusters of heterogeneities (Fig. 3 middle panel, and Fig. S1 of SM). The abrupt change in A and B is a static signature of a first-order-like PT. At high pressures, the predominance of B over A is restored in both HDA_{Ih} and HDA_{LDA} . This suggests that the large-scale density fluctuations are suppressed and are comparable with those in LDA. However, the large-scale structures of HDA_{Ih} and HDA_{LDA} slightly differ one from another at intermediate pressures, i.e., at $1.5 \lesssim p \lesssim 2.2$ GPa, but upon further compression, the coefficients A of both HDAs become almost identical (Fig. 1, inset), suggesting that HDA_{Ih} and HDA_{LDA} have similar large-scale structures. This observation is further reinforced by the similar values acquired by the coefficient B for both HDAs at $p \gtrsim 2.1$ GPa. To get deeper insight into the hyposurficiality and hyperuniformity of amorphous ices, we compute the translational order metric τ [5],

$$\tau = \frac{1}{(2\pi)^3 \rho^2 D^3} \int_0^\infty [S(\mathbf{k}) - 1]^2 d\mathbf{k}, \quad (5)$$

where D is a characteristic microscopic length scale. In the thermodynamic limit, τ diverges for perfect crystals while it vanishes identically for spatially uncorrelated systems. Thus, a deviation of τ from 0, which can only be positive, measures the degree of translational order relative to the fully uncorrelated case. In Fig. 2 we report τ for the compression of *Ih* (black) and LDA (red). Since *Ih*

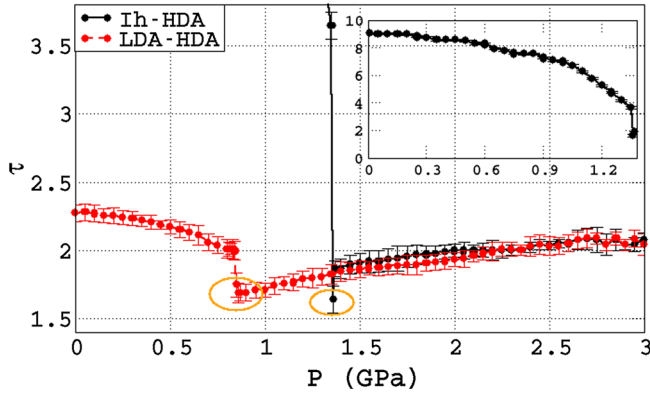


FIG. 2. Translational order metric τ during compression of *Ih* (black, continuous) and LDA (red, dashed). Sudden drops of τ occur in correspondence with the PTs. Inset: τ of *Ih* at low pressures.

possesses long-range order, large positive values of τ for *Ih* are removed from the main figure and are reported in the inset. This representation allows us to (i) emphasize the lower values of τ of LDA compared to *Ih*, and (ii) report the jump in τ in correspondence with both PTs. The finite values of τ for *Ih* are caused by the finite size of our sample, which causes a truncation of the upper integration limit in Eq. (5) [35]. For $p < p_T$, τ decreases continuously upon compression in both samples, as structural heterogeneities appear, which, at this stage, affect τ but are not concentrated enough to sensitively influence the values of A and B . In correspondence with the PTs, τ acquires its minimum values, indicating that some degree of decorrelation should be present. Moreover, τ shows a discontinuity, further indication of a first-order-like PT. After the PT, the τ 's of HDA_{Ih} and HDA_{LDA} differ slightly from one another for $1.5 \lesssim p \lesssim 2.2$ GPa. This difference is a further signature of structural differences at the large scale in HDA_{Ih} and in HDA_{LDA} . Upon further compression, such differences become negligible. Notably, the values of τ for both HDAs at high pressures ($p \sim 3.0$ GPa) are very close to the values of τ in LDA for $0.5 \lesssim p \lesssim 0.8$ GPa. This suggests that similar translational order is present in both amorphous structures, in contrast with the reported differences at small distances [19,33,36]. At small length scales, the local environment is tetrahedral with well-separated first and second shells of neighbors in LDA and *Ih*. By contrast, the environment is distorted in HDA, similar to liquid water at standard conditions, due to interstitial molecules populating the first intershell region [36]. In Fig. 3 we report representative snapshots and the corresponding $S(k)$ of the *Ih*-to-HDA transformation

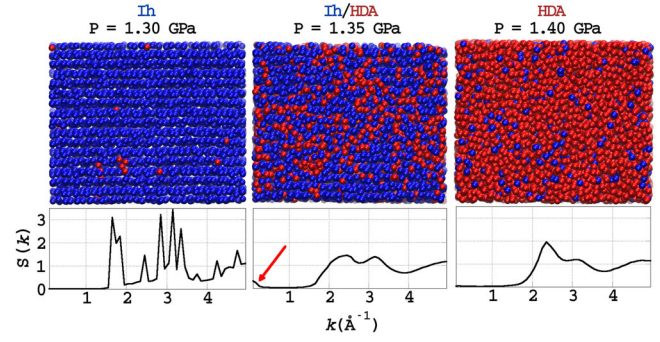


FIG. 3. Snapshots of representative configurations before (left), near (center), and after (right) the *Ih*-to-HDA transformation. Oxygen sites are represented by blue or red spheres, respectively, for *Ih* or HDA character based on the local structure index. The corresponding $S(k)$ is reported below each snapshot.

presence of interstitial molecules in the intershell region. It is noteworthy that, before the transition, $S(k)$ exhibits crystalline Bragg peaks that disappear in the disordered structures of the middle and right panels. However, while the HDA structure on the right is nearly hyperuniform, the $S(k)$ of the middle panel displays a characteristic $k \sim 0$ feature (indicated by the arrow) associated to large-scale density fluctuations. A similar picture holds for the LDA-to-HDA transformation.

We quantify the hyperuniformity of the system by calculating the ratio $H = S(0)/S(k_{\text{peak}})$. Figure 4(a) reports H for the compression of *Ih* (black) and LDA (red).

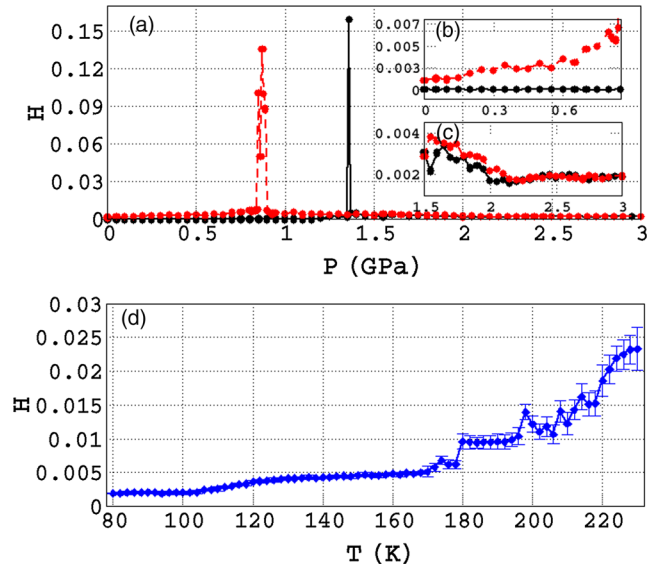


FIG. 4. (a) $H = S(0)/S(k_{\text{peak}})$ during compression of *Ih* (black, continuous) and LDA (red, dashed). The peaks in correspondence with the PTs (*Ih* to HDA and LDA to HDA) reach values that are 2 orders of magnitude larger than the qualitative threshold for hyperuniformity ($H \sim 10^{-3}$). (b) Zoom of H before the LDA-to-HDA PT. (c) Zoom of H after the *Ih*-to-HDA PT. (d) H during cooling of liquid water down to $T = 80$ K at $p = 0.1$ GPa. Averages are taken over 10 independent runs.

Figure 4(b) shows that Ih has $H \sim 10^{-4}$ before the PT, and is, therefore, close to perfect hyperuniformity, whereas LDA has H ranging from $\sim 2 \times 10^{-3}$ to $\sim 6 \times 10^{-3}$, signaling that it is nearly hyperuniform. The degree of hyperuniformity continuously decreases with increasing pressure, due to the appearance of HDA-like sites representing structural heterogeneities. In correspondence with the PTs, heterogeneities suppress the hyperuniformity, as indicated by the spikes of H . At $p > p_T$, HDAs are produced and their values of H are shown in Fig. 4(c). Both HDAs are nearly hyperuniform, with H ranging from $\sim 4 \times 10^{-3}$ to $H \sim 2 \times 10^{-3}$ with increasing pressure. The large-scale structures of the two amorphous ices, which differ slightly for $p < 2.2$ GPa, become quite similar above 2.2 GPa. At these high pressures the degree of hyperuniformity of the HDAs is similar to that of LDA at low pressure. Note that LDA and HDA have different hydrogen bond networks (HBNs). The HBN of LDA is dominated by five-, six-, and sevenfold rings, in contrast to HDA, whose HBN includes a significant fraction of longer member rings to accommodate the larger density [39]. Despite these differences, each water molecule is almost perfectly fourfold coordinated in LDA and HDA [39]. Therefore, the nearly hyperuniform nature of LDA and of HDA indicates that the HBNs of both amorphous ices belong to the class of nearly hyperuniform bond networks [10], i.e., isotropic networks lacking of crystallinity and coordination defects, in which all particles are perfectly coordinated, forming continuous random networks (CRNs), enriched with the suppression of large-scale density fluctuations.

The structure factor of an equilibrium liquid in the infinite-wavelength limit is related to the isothermal compressibility κ_T via $\lim_{k \rightarrow 0} S(k) = \rho k_B T \kappa_T$, where ρ is the density and k_B is the Boltzmann constant. The liquid $S(k)$ displays a positive curvature for small wave vectors [40–43]. In our liquid water model at $T = 300$ K $H \sim 0.07$ and progressively decreases with cooling down to the supercooled regime [Fig. 4(d)]. For this model, at the adopted cooling rate, the glass transition occurs at $T_{\text{gr}} \approx 200$ K [19]. In the temperature range $196 < T < 204$ K, $H \sim 0.011$ indicating that, in correspondence with the freezing of the translational degrees of freedom, the system is still not hyperuniform. Large-scale density fluctuations keep occurring as the sample is cooled down to $T_{\text{gr}} \sim 180$ K, the temperature of the freezing of molecular rotational degrees of freedom. We attribute the large-scale density fluctuations in the range $T_{\text{gr}} \lesssim T \lesssim T_{\text{gr}}$ mainly to changes of the HBN due to bond switches caused by the molecular rotations [44]. Molecular diffusion is instead the main contributor for $T > T_{\text{gr}}$. Upon further cooling, the large-scale density fluctuations drop rapidly to $H \sim 0.006$ below T_{gr} and then keep decreasing, until they saturate to $H \sim 0.002$ for $T \sim 100$ K Fig. 4(d). The continuous decrease of fluctuations for $T \lesssim T_{\text{gr}}$ does not involve any

rearrangement of the HBN. It is due instead to the varying amplitude of the vibrational motions as well as to small local displacements of the molecules that reflect the anharmonicity of the potential in the glass and conspire to suppress the large-scale density fluctuations when the CRN is fully formed. The structural changes revealed by the substantial reduction of H for $T < T_{\text{gr}}$ indicate that LDA is not simply a structurally arrested liquid.

The quantity A/B is the ratio of volume to surface-area fluctuations and is a useful metric to detect the emergence of hyperuniformity or hyposurficiality at thermodynamic conditions away from criticality; at criticality, this ratio becomes meaningless. As shown in Fig. S2 of the SM, we find that nearly hyperuniform states occur when $A/B < 0.015$.

Conclusions.—By analyzing the long wavelength density fluctuations of LDA and HDA generated with classical molecular dynamics simulations, we found that both amorphous ices are nearly hyperuniform and have a similar degree of hyperuniformity. This suggests that they should possess similar long-range order in spite of their clear differences at the short- and intermediate-range scales independently of the preparation protocol followed to produce HDA. In correspondence with the transformation of Ih to HDA and of LDA to HDA, the applied pressure produces clusters of spatially nearly uncorrelated heterogeneities that destroy hyperuniformity. When this occurs, the samples become hyposurficial as density fluctuations that grow like the surface area of the observation window are absent. Hyposurficiality is a static signature that should be inspected whenever a first-order PT is involved, which, to our knowledge, was never previously observed as a signature of phase coexistence in any context. The sudden appearance of hyposurficiality, the discontinuous profile of the translational order metric τ , and the spike of H in correspondence with the PTs, lead us to conclude that the observed Ih -to-HDA and LDA-to-HDA transformations are of the first kind. The first-order nature of the LDA-to-HDA metastable phase transition makes conceivable the existence of a second critical point in our model of water.

An additional important finding of our investigation is that the large-scale density fluctuations keep decreasing well below T_{gr} and T_{gr} , i.e., well below the temperature of freezing of diffusional and rotational motion, challenging the notion of glasses as kinetically arrested liquids. Our results also indicate that the degree of hyperuniformity of a glass is affected by vibrational motion and, in particular, that not all glasses are hyperuniform.

Finally, we propose that away from criticality, the ratio A/B could provide a useful metric to gauge the degree of volume to surface-area fluctuations, which include hyperuniform and hyposurficial systems at the extremes.

F. M. and R. C. acknowledge the Department of Energy (DOE), Award No. DE-SC0008626. S. T. was supported by the National Science Foundation under Award No. DMR-1714722.

*Corresponding author.

faustom@princeton.edu

- [1] S. Torquato and F. H. Stillinger, *Phys. Rev. E* **68**, 041113 (2003).
- [2] See Supplemental Material at <http://link.aps.org/supplemental/10.1103/PhysRevLett.119.136002> for the mathematical definition of $\alpha(\mathbf{r}, R)$ and for additional analyses of the simulation.
- [3] C. E. Zachary and S. Torquato, *J. Stat. Mech.* (2009) P12015.
- [4] Upon ensemble average over many configurations, one can average $h(\mathbf{r})$ over orientations of \mathbf{r} obtaining a total correlation function that depends on $r = |\mathbf{r}|$. Moreover, it is worthy to note that the definition in Eq. (3) removes any forward scattering contribution, which is always omitted in the definition of hyperuniformity.
- [5] S. Torquato, G. Zhang, and F. H. Stillinger, *Phys. Rev. X* **5**, 021020 (2015).
- [6] A. Donev, F. H. Stillinger, and S. Torquato, *Phys. Rev. Lett.* **95**, 090604 (2005).
- [7] Y. Jiao, T. Lau, H. Hatzikirou, M. Meyer-Hermann, J. C. Corbo, and S. Torquato, *Phys. Rev. E* **89**, 022721 (2014).
- [8] L. Pietronero, A. Gabrielli, and F. S. Labini, *Physica (Amsterdam)* **306A**, 395 (2002).
- [9] R. Xie, G. G. Long, S. J. Weigand, S. C. Moss, T. Carvalho, S. Roorda, M. Hejna, S. Torquato, and P. J. Steinhardt, *Proc. Natl. Acad. Sci. U.S.A.* **110**, 13250 (2013).
- [10] M. Hejna, P. J. Steinhardt, and S. Torquato, *Phys. Rev. B* **87**, 245204 (2013).
- [11] M. Florescu, S. Torquato, and P. J. Steinhardt, *Proc. Natl. Acad. Sci. U.S.A.* **106**, 20658 (2009).
- [12] W. Man, M. Florescu, E. P. Williamson, Y. He, S. R. Hashemizad, B. Y. C. Leung, D. R. Liner, S. Torquato, P. M. Chaikin, and P. J. Steinhardt, *Proc. Natl. Acad. Sci. U.S.A.* **110**, 15886 (2013).
- [13] G. Zito, G. Rusciano, G. Pesce, A. Malafronte, R. Girolamo, G. Ausanio, A. Vecchione, and A. Sasso, *Phys. Rev. E* **92**, 050601(R) (2015).
- [14] A. Chremos and J. F. Douglas, *Ann. Phys. (Amsterdam)* **529**, 1600342 (2017).
- [15] G. Zhang, F. H. Stillinger, and S. Torquato, *Sci. Rep.* **6**, 36963 (2016).
- [16] T. Goldfriend, H. Diamant, and T. A. Witten, *Phys. Rev. Lett.* **118**, 158005 (2017).
- [17] S. Atkinson, G. Zhang, A. B. Hopkins, and S. Torquato, *Phys. Rev. E* **94**, 012902 (2016).
- [18] J. L. F. Abascal and C. Vega, *J. Chem. Phys.* **123**, 234505 (2005).
- [19] J. Wong, D. A. Jahn, and N. Giovambattista, *J. Chem. Phys.* **143**, 074501 (2015).
- [20] O. Mishima and L. D. Calvert, *Nature (London)* **310**, 393 (1984).
- [21] O. Mishima, L. D. Calvert, and E. Whalley, *Nature (London)* **314**, 76 (1985).
- [22] K. Koga, H. Tanaka, and X. C. Zeng, *Nature (London)* **408**, 564 (2000).
- [23] S. Klotz, T. Strässle, G. Hamel, R. J. Nelmes, J. S. Loveday, G. Hamel, G. Rouse, B. Canny, J. C. Chervin, and A. M. Saitta, *Phys. Rev. Lett.* **94**, 025506 (2005).
- [24] J. L. F. Abascal and C. Vega, *J. Chem. Phys.* **133**, 234502 (2010).
- [25] R. S. Singh, J. W. Biddle, M. A. Anisimov, and P. G. Debenedetti, *J. Chem. Phys.* **144**, 144504 (2016).
- [26] P. G. Debenedetti, *J. Phys. Condens. Matter* **15**, R1669 (2003).
- [27] T. Loerting and N. Giovambattista, *J. Phys. Condens. Matter* **18**, R919 (2006).
- [28] O. Mishima and H. E. Stanley, *Nature (London)* **396**, 329 (1998).
- [29] T. Loerting, V. Fuentes-Landetea, P. H. Handlea, M. Seidl, K. Amann-Winkel, C. Gainaru, and R. Bohme, *J. Non-Cryst. Solids* **407**, 423 (2015).
- [30] K. Amann-Winkel, R. Bohmer, F. Fujara, C. Gainaru, B. Geil, and T. Loerting, *Rev. Mod. Phys.* **88**, 011002 (2016).
- [31] T. Loerting, C. Salzmann, I. Kohl, E. Mayer, and A. Hallbrucker, *Phys. Chem. Chem. Phys.* **3**, 5355 (2001).
- [32] C. A. Tulk, C. J. Benmore, L. Urquidi, D. D. Klug, J. Neufeing, B. Tomberli, and P. A. Egelstaff, *Science* **297**, 1320 (2002).
- [33] J. L. Finney, A. Hallbrucker, I. Kohl, A. K. Soper, and D. T. Bowron, *Phys. Rev. Lett.* **88**, 225503 (2002).
- [34] K. Winkel, E. Mayer, and T. Loerting, *J. Phys. Chem. B* **115**, 14141 (2011).
- [35] The upper integration limit is defined by the reciprocal vectors associated to the natural periodicity of I_h in units of the reciprocal lattice vectors of the sample supercell.
- [36] A. K. Soper and M. A. Ricci, *Phys. Rev. Lett.* **84**, 2881 (2000).
- [37] E. Shiratani and M. Sasai, *J. Chem. Phys.* **104**, 7671 (1996).
- [38] E. Shiratani and M. Sasai, *J. Chem. Phys.* **108**, 3264 (1998).
- [39] R. Martoňák, D. Donadio, and M. Parrinello, *J. Chem. Phys.* **122**, 134501 (2005).
- [40] J. A. Sellberg *et al.*, *Nature (London)* **510**, 381 (2014).
- [41] K. T. Wikfeldt, A. Nilsson, and L. G. M. Pettersson, *Phys. Chem. Chem. Phys.* **13**, 19918 (2011).
- [42] D. Dhabal, K. T. Wikfeldt, L. B. Skinner, C. Chakravarty, and H. K. Kashyap, *Phys. Chem. Chem. Phys.* **19**, 3265 (2017).
- [43] G. N. I. Clark, C. R. Cappa, J. D. Smith, R. J. Saykally, and T. Head-Gordon, *Mol. Phys.* **108**, 1415 (2010).
- [44] F. Martelli, H.-Y. Ko, E. C. Oğuz, and R. Car, arXiv:1609.03123.